

# Effect of Localized Corrosion on Fatigue–Crack Growth in 2524-T3 and 2198-T851 Aluminum Alloys Used as Aircraft Materials

J.A. Moreto, E.E. Broday, L.S. Rossino, J.C.S. Fernandes, and W.W. Bose Filho

(Submitted September 12, 2017; in revised form December 5, 2017; published online March 1, 2018)

Corrosion and fatigue of aluminum alloys are major issues for the in-service life assessment of aircraft structures and for the management of aging air fleets. The aim of this work was to evaluate the effect of localized corrosion on fatigue crack growth (FCG) resistance of the AA2198-T851 Al-Li alloy (Solution Heat Treated, Cold Worked, and Artificially Aged), comparing it with the FCG resistance of AA2524-T3 (Solution Heat Treated and Cold Worked), considering the effect of seawater fog environment. Before fatigue tests, the corrosion behavior of 2198-T851 and 2524-T3 aluminum alloys was verified using open circuit potential and potentiodynamic polarization techniques. Fatigue in air and corrosion fatigue tests were performed applying a stress ratio ( $R$ ) of 0.1, 15 Hz (air) and 0.1 Hz (seawater fog) frequencies, using a sinusoidal waveform in all cases. The results showed that the localized characteristics of the 2198-T851 and 2524-T3 aluminum alloys are essentially related to the existence of intermetallic compounds, which, due to their different nature, may be cathodic or anodic in relation to the aluminum matrix. The corrosive medium has affected the FCG rate of both aluminum alloys, in a quite similar way. Graphical Abstract

**Keywords** Al alloys, corrosion–fatigue, seawater fog environment, 2XXX series Al alloys

## 1. Introduction

Aluminum (Al) is a widely used nonferrous metal, and it competes with various materials, since it offers low cost and many other competitive advantages (Ref 1). Among the properties that make Al an attractive metal for structural applications in aircrafts is its low density. Al could be “ideal” if it was possible to combine the low density with a high mechanical resistance, which does not happen, at least, in the pure Al. The way to improve its mechanical resistance is by

adding alloying elements, such as Cu, Mg, Si, and Li among others. Al has good corrosion resistance due to the stability of oxide film that forms on the surface; however, the introduction of alloying elements and the consequent formation of precipitates lead to the loss of this resistance, the material being very sensitive to the corrosion process. The unique combination of chemical and mechanical properties gives a wide range of Al alloys applications, especially in the transport, construction, packaging, and energy fields.

On the other side, the aircraft industry leads the search for improved materials that offer benefits in terms of improved mechanical and corrosion performances, associated with weight and cost savings (Ref 2). The 2XXX series Al alloys have copper (Cu) as main alloying element, and the main characteristics of this family are: higher strength (at T6 temper), reduced FCG rate (at T4 temper), thermal resistance, and easy machinability (Ref 3). This series is commonly used in aircraft applications where high strength-to-weight ratios are required. The AA2198-T851 belongs to the third generation of the Al-Cu-Li family (Ref 4), whose development was based on weight reduction, since it presents lower density, higher strength, and toughness than other Al alloys from this series. This alloy contains lithium (Li) as an alloying element, which reduces its density, and at same time, increases the Young’s modulus, leading to weight saving. In fact, the addition of 1 wt.% Li to aluminum reduces the alloy’s density by 3% and increases its elastic modulus by 6% (Ref 5). Owing to their high strength and low density, the Al-Cu-Mg-based 2XXX series of aluminum alloys, such as the AA2524, are widely used for constitutive aircraft parts; hence, damage tolerance is a critical issue (Ref 6). This alloy was developed by the Aluminum Company of America (ALCOA) in the 1990s by adjusting the Cu and Mg alloying elements and reducing Fe and Si levels (Ref 7).

**J.A. Moreto**, Institute of Exact Sciences, Naturals and Education, Federal University of Triângulo Mineiro (UFTRM), Avenida Doutor Randolfo Borges Júnior, Univerdecidade, Uberaba, Minas Gerais 38064200, Brazil; and Department of Materials Engineering, University of São Paulo, Av. Trabalhador São-carlense, São Carlos, SP 13566590, Brazil; **E.E. Broday**, Department of Production Engineering, Federal University of Technology of Paraná (UTFPR), Av. Monteiro Lobato s/n Km 04, Ponta Grossa, PR 84016-210, Brazil; **L.S. Rossino**, Sorocaba Technological College (FATEC), Av. Engenheiro Carlos Reinaldo Mendes, Alto da Boa Vista, Sorocaba, São Paulo 18013-280, Brazil; and Federal University of São Carlos - UFSCar, Rodovia João Leme dos Santos Km 110, Bairro do Itinga, 18.052-780, Sorocaba, SP, Brazil; **J.C.S. Fernandes**, Department of Chemical Engineering, Instituto Superior Técnico, University of Lisbon, 1049-001 Lisbon, Portugal; and CQE - Centro de Química Estrutural, 1049-001 Lisbon, Portugal; and **W.W. Bose Filho**, Department of Materials Engineering, University of São Paulo, Av. Trabalhador São-carlense, São Carlos, SP 13566590, Brazil. Contact e-mail: jeferson.moreto.uftrm@gmail.com.

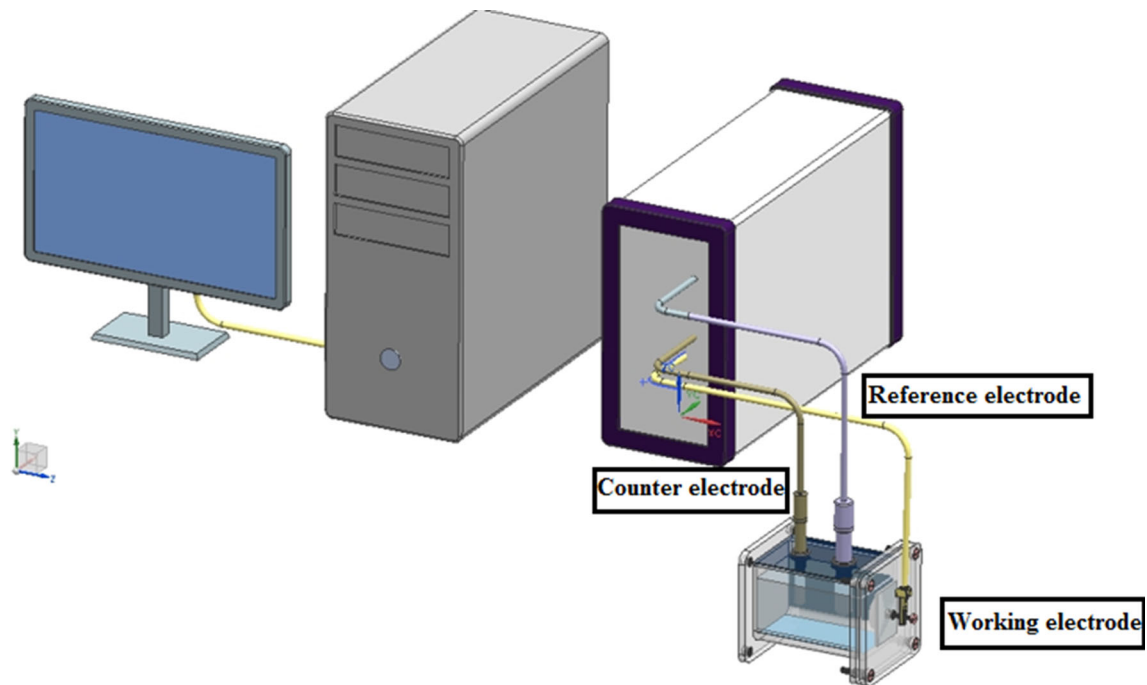


**Fig. 1** Electrochemical apparatus for corrosion tests. *Source:* Author

Several factors influence the fatigue life of aluminum alloys; among them, it can be mentioned: the average tension ( $\sigma_m$ ) normally varying in terms of load ratio  $R$ , the fracture toughness of the material, the thickness, the microstructure, surface finishing, loading modes, waveform, frequency, presence of corrosive media, and crack closure phenomenon. Both nucleation and growth rate can be significantly influenced by the environment. However, it is difficult to quantify its effect due to the large number of mechanical, metallurgical, and chemical variables present and the interaction among them. Furthermore, other additional factors influencing on the effect of the environment are loading frequency, test temperature, and waveform (Ref 8). Corrosion fatigue (CF) occurs in metals as a result of the combined action of a cyclic stress and a corrosive environment. CF is dependent on the interactions among loading, environmental, and metallurgical factors. In general, an aggressive environment causes a decrease in the fatigue resistance of a component, affecting the probability of crack initiation by fatigue, FCG rate, or both (Ref 9).

The reduction in fatigue life of aircraft components may become significant by the presence of aggressive saline media. The understanding of the corrosion-fatigue phenomena, kinetics, and micromechanisms acting is essential for life prediction, as well as for the development of alloys with increased fatigue performance. The aim of this work was to study the localized corrosion on the fatigue crack growth rate of the AA2198-T851 Al-Li alloy (from the third generation), taking the AA2524-T3 as a baseline, considering the effect of a 3.5 wt.% seawater fog environment.

## 2. Experimental

The materials used in this investigation were the AA2524-T3 (considered as the base alloy) produced by ALCOA and the

AA2198-T851 (Al-Li alloy) produced by Rio Tinto Alcan, both provided as 1.6 mm sheets in the bare condition (without any cladding or other surface treatment). The chemical composition analysis carried out by Moreto (Ref 10) and presented elsewhere has shown that the values are in accordance with the recommendations.

The open circuit potential (OCP) and potentiodynamic polarization (PP) curves were obtained in aerated 0.6 mol L<sup>-1</sup> sodium chloride (NaCl) solution. A Gamry 600 potentiostat/galvanostat was used for the electrochemical tests. For this purpose, an electrochemical cell containing a single compartment of three electrodes was used: AA2198-T851 and AA2524-T3 aluminum alloys as working electrode (WE), a Pt foil as counter electrode (CE) and reference electrode (RE) of saturated calomel Hg/Hg<sub>2</sub>Cl<sub>2</sub>, KCl<sub>sat</sub>. OCP measurements were performed for both aluminum alloys for a period of 600 s. The PP measurements were carried out in triplicate using a scan rate of 0.5 mV s<sup>-1</sup>. The potential range used was 00 to -1.4 V. Before each electrochemical tests, the samples with a geometric area of 0.38 cm<sup>2</sup> were mechanically polished (120–4000#), washed in distilled water, and then degreased in propanol for a period of 10 min. All the electrochemical experiments were performed at 25 ± 2 °C. Figure 1 shows the apparatus used for the electrochemical tests.

Tensile tests were performed in air and at room temperature followed the ASTM E8 M standard (Ref 11) with a displacement rate of 1 mm min<sup>-1</sup>, corresponding to a nominal deformation rate of 6.7 × 10<sup>-5</sup> mm s<sup>-1</sup>. The elongation measurements were performed using an extensometer with a gage length of 25 mm. The geometry and dimensions of the tensile specimens are shown in Fig. 2. The tensile tests were used to quantify the monotonic properties of the studied alloys: yield strength ( $\sigma_{0.2\%}$ ), ultimate tensile strength (UTS), and total elongation (EI%).

Aiming the observation of the deleterious effects of a seawater fog environment on the fatigue crack growth (FCG)

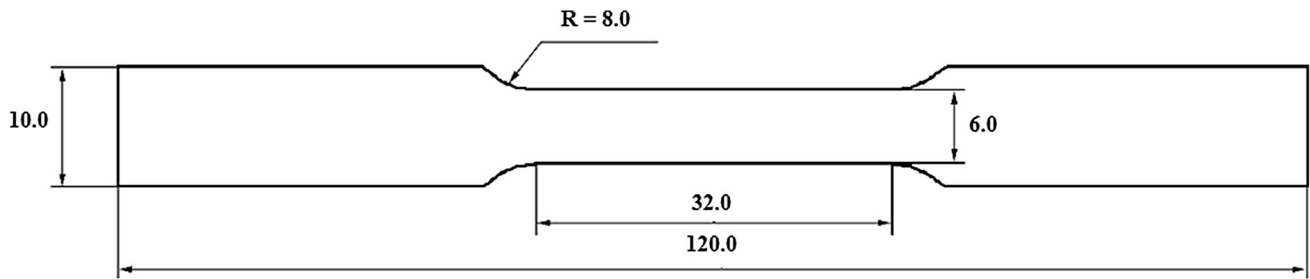


Fig. 2 Size and geometry of the dog bone specimen (dimensions in mm). ASTM E8 M-00 (Ref 11). Source: Author

rate, fatigue tests were carried out following the ASTM E647-11 (Ref 12), in a 100 kN capacity MTS servo-hydraulic testing system, under load control, sinusoidal waveform, frequencies of 15 Hz (air) and 1 Hz (saline environment), stress ratio,  $R = 0.1$ , room temperature (RT), and in seawater fog (water solution with 3.5 wt.% NaCl). In all cases, fatigue precracking was conducted in air, at 15 Hz frequency and to a minimum crack size of 1 mm from the notch tip. Figure 3 shows the size and geometry of the M (T) specimen type, removed in the T–L direction. The fatigue tests data were stored in a microcomputer and then processed in specific graphics programs, where the parameters of the Paris–Erdogan equation ( $A$  and  $m$ ) for each case were obtained.

In seawater fog at RT, the tests followed similar procedure applied in air. A special acrylic cell and a reservoir for fog generation were specially fabricated. In this setup, the seawater fog circulated through the cell, supplied by the external reservoir and then expelled to the external environment, details may be verified in Fig. 4 (Ref 13). The fatigue threshold,  $\Delta K_{th}$ , was evaluated for the both Al alloys considering only the air environment. In this case, as recommended by the ASTM E647-11 (Ref 12), the tests were carried out in K control. The above requirements can be met by limiting the normalized K gradient,  $C = (1/K) dK/da$ , to a value algebraically equal to or greater than  $-0.08 \text{ mm}^{-1} (-2 \text{ in}^{-1})$ , that is:

$$C = \frac{1}{k} \left( \frac{dK}{dN} \right) > -0,08 \text{ mm}^{-1} (-2 \text{ in}^{-1}) \quad (\text{Eq 1})$$

When forces are incrementally shed, the requirements on  $C$  correspond to the nominal K gradient. According to ASTM B909 (2000) (Ref 13) and Hudak et al. (Ref 14), acceptable values of  $C$  may depend on load ratio, test material, and environment. Values of  $C$  algebraically greater than those indicated above have been demonstrated as acceptable for use in decreasing  $K$  tests of several steel alloys and Al alloys tested in laboratory air over a wide range of force ratios. Since crack growth was monitored by electric potential drop technique, it was not possible to get the threshold values for the saline fog environment.

Otherwise, the FCG tests were carried out in load control. FCG tests were used to determine the threshold stress intensity starting from  $\Delta K = 8 \text{ MPa m}^{1/2}$  and  $C = -0.078 \text{ mm}^{-1}$ . In the seawater fog, crack size was determined by electric potential drop technique (EPD), as described in detail elsewhere (Ref 10). The chemical composition of the seawater fog used was 3.5%wt NaCl. The parameters used in this test were determined experimentally. It is important to note that during the determination of these parameters, the pressure was adjusted to 45 Psi. The chamber to store saline solution was designed for a volume

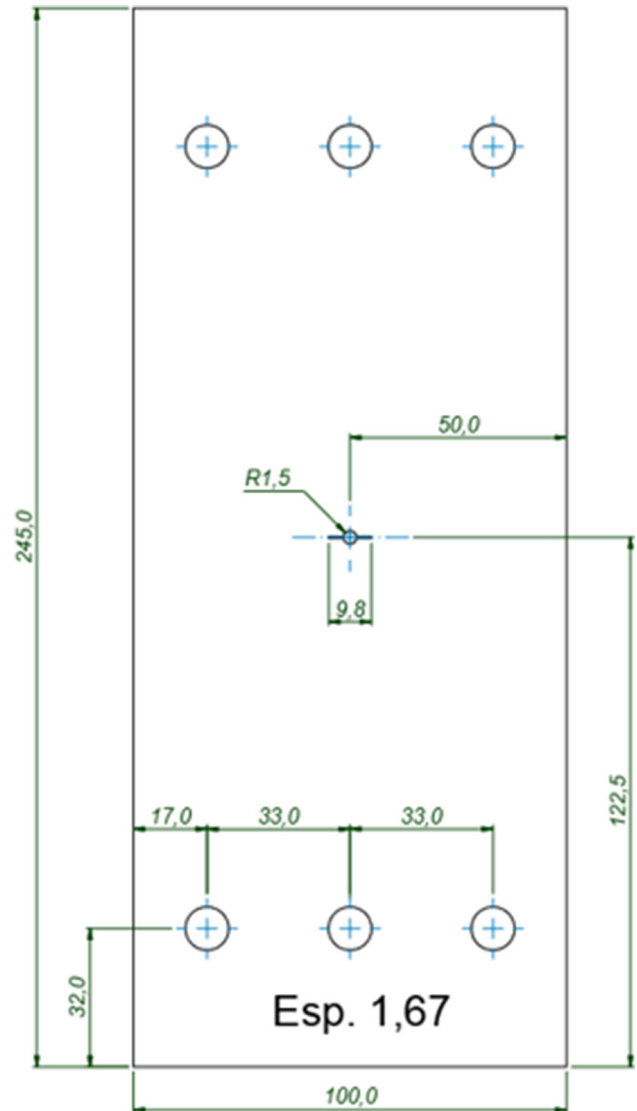


Fig. 3 Size and geometry of the T-L laboratory specimen (dimensions in mm). ASTM E647-11 (Ref 12). Source: Author

of approximately 3 L of solution. Thus, the liquid solution was pressurized in 45 Psi and the fog formed was conducted by the pipe to the chamber surrounding the specimen. Figure 4 schematically shows how the fatigue tests in seawater fog environment were conducted. The reading wires were protected by resin so that they did not suffer corrosion due to the presence of seawater fog. The potentiostat equipment used is the Agilent

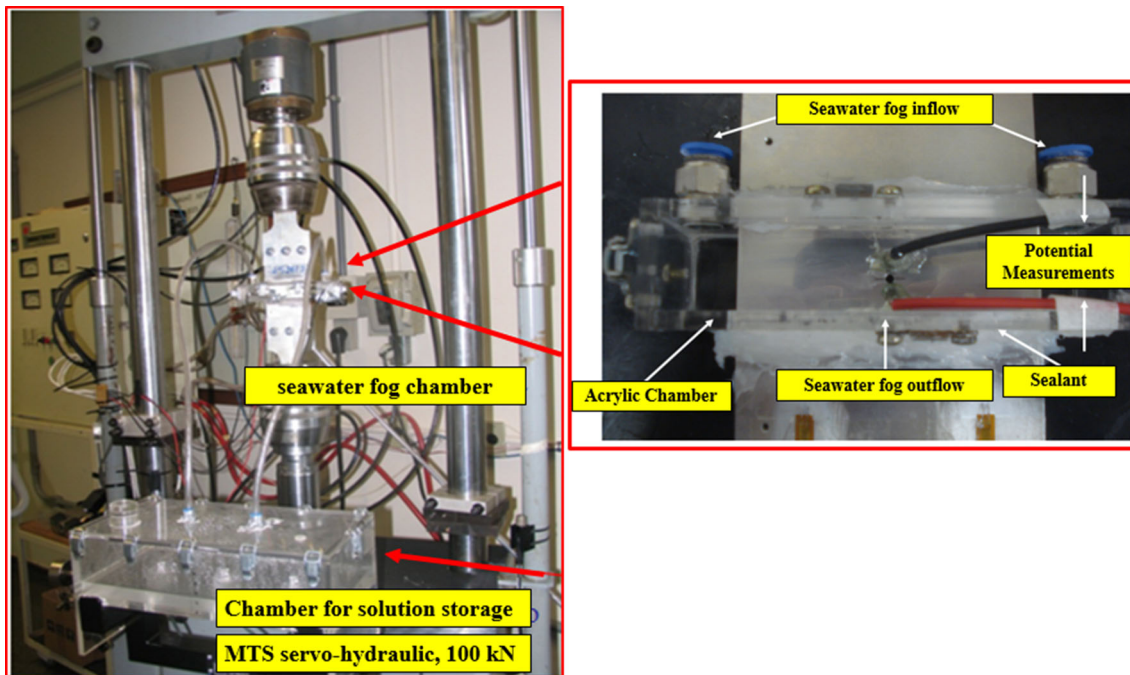


Fig. 4 Schematic view of the experimental setup for corrosion fatigue tests. Source: Author

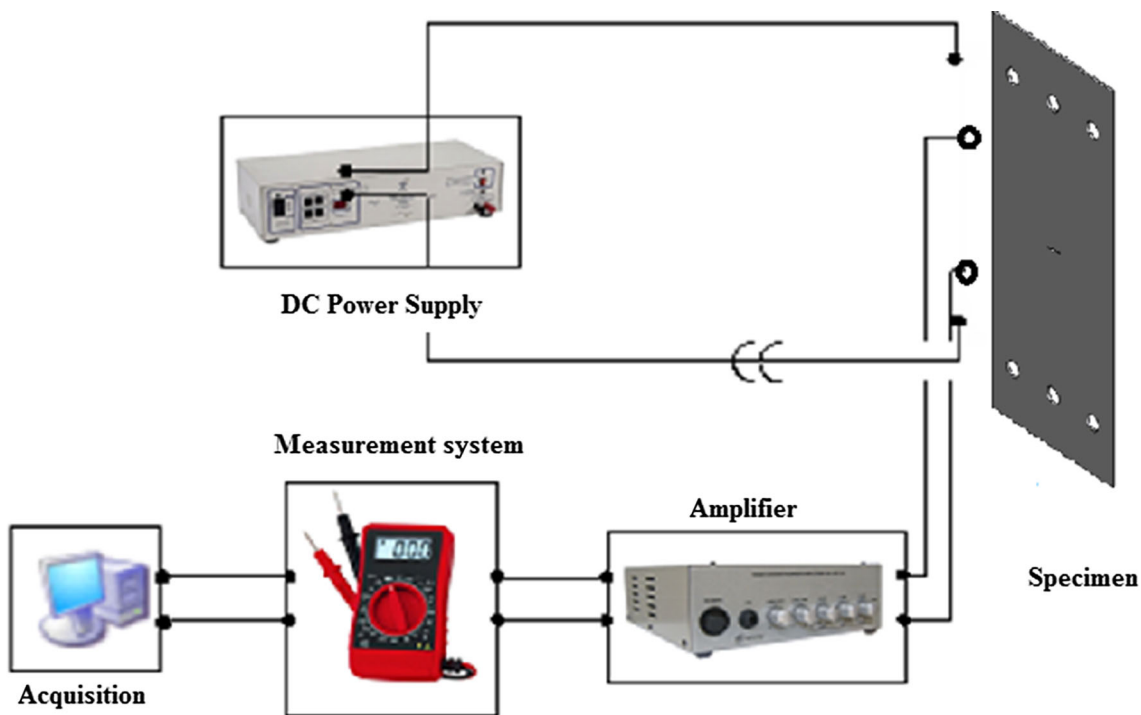


Fig. 5 Settings for FCG tests in saline fog using the potential drop technique. Source: Author

brand, model 6651 A 0–8 V/0–50 A and nanovoltmeter model 34420A. Figure 5 schematically shows the M (T) specimen assembly for performing the FCG tests using the EPD technique.

According to ASTM E 647-11 (ASTM, 2011) (Ref 12), the crack size of a M(T) type specimen can be determined by the EPD recorded during tests, according to the procedure previously described elsewhere (Ref 10). The relationship between crack size,  $a$ , and potential drop,  $V$ , follows below:

$$a = \frac{W}{\pi} \cos^{-1} \left[ \frac{\cosh\left(\frac{\pi}{W} x Y_0\right)}{\cosh\left(\frac{V}{V_r} x \cosh^{-1}\left(\frac{\cosh\left(\frac{\pi}{W} x Y_0\right)}{\cos\left(\frac{\pi}{W} x a_r\right)}\right)\right)} \right], \quad (\text{Eq 2})$$

where  $a$  represents the crack size,  $a_r$  the reference crack size,  $W$  the width of sample,  $V$  the measured variation in the elec-

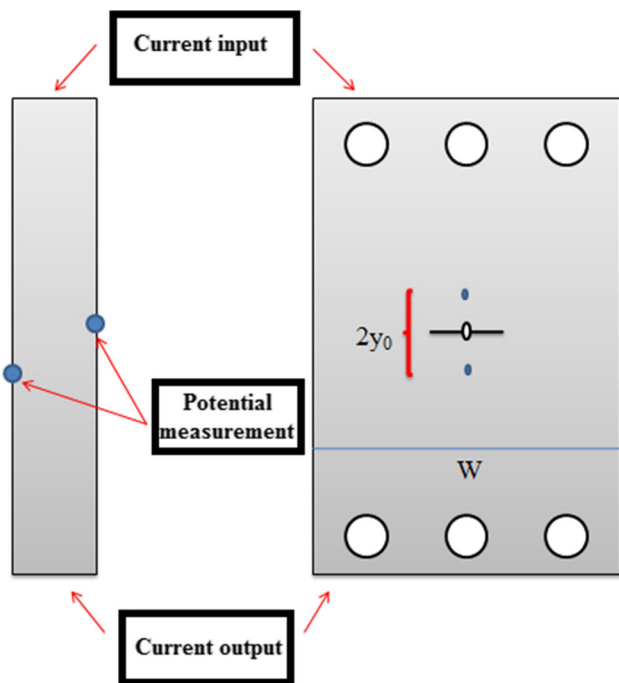


**Fig. 6** Wire assembling for electric potential drop measurement in M (T) type specimen following the ASTM E647-11 (Ref 12). Source: Author

tric potential,  $V_r$  the electric potential difference measured when crack size is  $a_r$ , and  $Y_0$  the distance from the point where the potential is being measured and the crack plane.

This relationship is valid only in cases where the current density is uniform at some remote cross section from the crack plane and the voltage is measured on the centerline of the specimen across the crack plane as can be seen in Fig. 6 (Ref 12). The incremental polynomial method was used to obtain the FCG rate curves  $da/dN$  versus  $\Delta K$ . Based on this method and in its algorithm described by ASTM E647 (ASTM, 2011) (Ref 12), a computer program was developed to perform evaluations of  $da/dN$  and the corresponding  $\Delta K$ . After the fatigue tests, the samples fracture surfaces were analyzed and both the mean size of the fatigue precrack and final crack size were obtained and the  $da/dN \times \Delta K$  curves were corrected. Finally, the fatigue crack surface was analyzed by scanning electron microscopy (SEM).

### 3. Results and Discussion

#### 3.1 Open Circuit Potential and Potentiodynamic Polarization Measurements

Figure 7(a) shows the OCP curves for the AA2198-T851 and AA2524-T3 aluminum alloys over a period of 600 s, preceded by potentiodynamic polarization tests. The values of  $E_{\text{corr}}$  obtained in the present work were  $-0.71 \pm 0.0160$  V (AA2198-T851) and  $-0.59 \pm 0.0049$  V (AA2524-T3). Figure 7 (b) and (c) illustrates the PP curves of the AA2198-T851 and AA2524-T3 aluminum alloys under study. As can be seen in the figures, the  $E_{\text{corr}}$  and pit potential ( $E_{\text{pit}}$ ) values are very similar, indicating that neither of the 2xxx series aluminum alloys presented passivation behavior. It is possible to argue that the AA2198-T851 alloy has  $E_{\text{corr}}$  lower than the AA2524-

T3 alloy, indicating a worse corrosion behavior. However, the cathodic activity (cathodic current) is higher for the AA2524-T3 alloy, which may indicate that this alloy has more precipitates acting as cathodes, therefore, causing a greater corrosion in the boundary zones. With regard to OCP curves, the lithium element shifts the corrosion potential values of the 2198 alloy for more negative values.

#### 3.2 Tensile Tests

Table 1 shows the mean and standard deviation of five tensile tests results performed for each alloy, according to ASTM E8M (Ref 11). The AA2198-T851 (Al-Cu-Li) (Solution Heat Treated, Cold Worked, and Artificially Aged) alloy when compared with AA2524-T3 (Solution Heat Treated and Cold Worked) presents superior performance in terms of yield strength and ultimate tensile strength. Cavaliere et al. (Ref 15) found similar values to those obtained in this work for the AA2198-T851 alloy, namely:  $\sigma_y = 436$  MPa,  $\sigma_{\text{LRT}} = 490$  MPa, and  $E = 74$  GPa. Souza et al. (Ref 16) also presented similar results for the AA2524-T3 aluminum alloy,  $\sigma_y = 337$  MPa,  $\sigma_{\text{LRT}} = 445$  MPa.

#### 3.3 Fatigue Crack Growth Tests in Air and Seawater Fog

The fatigue crack growth threshold is a value that depends on several factors: material type, loading ratio, R, and environment conditions. The  $\Delta K_{\text{th}}$  is the asymptotic value of  $\Delta K$  where the rate of  $da/dN$  tends to zero. By convention, this rate value may be considered null when the crack growth rate is close to  $10^{-7}$  mm/cycle. Six trials were performed to obtain  $\Delta K_{\text{th}}$  in air, being three for each alloy. Values of  $\Delta K_{\text{th}}$  were estimated using a linear regression of the  $da/dN$  versus  $\Delta K$  curve using at least five equally spaced points between the rates of  $10^{-6}$  and  $10^{-7}$  mm/cycle according to ASTM E – 647 (Ref 12). It was observed that the values of  $\Delta K_{\text{th}}$  were approximately 2.8 and 1.7 MPa  $\text{m}^{1/2}$ , respectively, for AA2198-T851 and AA2524-T3, with the latter presenting a slightly lower value.

The  $da/dN$  versus  $\Delta K$  relationship may be complex (Ref 17-19). In the linear region, FCG rates are defined by the linear elastic fracture mechanisms stress intensity factor range that combines the effects of applied load, crack size, and geometry (Ref 15). Figure 8(a) and (b) presents  $da/dN$  versus  $\Delta K$  curves for region II for both alloys, considering air and seawater fog environments. Comparing the FCG rate curves for the two materials tested in air, it is observed that the AA2524-T3 presents better fatigue resistance with lower  $m$  value and this difference increases with increasing  $\Delta K$ . As observed by Chen et al. (Ref 20), inclusions affect significantly the FCG rate of Al alloys. They proposed a FCG model considering that during fatigue tests, the debonded interfaces of inclusions produce substantial voids in the alloy, and these voids coalesce and serve as bridging during crack propagation. From the tensile test results, it is observed that the AA2524-T3 strain hardens more than the AA2198-T851, and this may enhance a better resistance to FCG, as observed by Tzamtzis and Kermanidis (Ref 21).

Paris-Erdogan Eq 3 is an effective approach to model FCG, and it may be written as follows:

$$\frac{da}{dN} = A \Delta K^m, \quad (\text{Eq 3})$$

where  $\Delta K$  is the stress intensity factor range,  $da/dN$  represents the fatigue crack growth rate, and  $A$  and  $m$  are material constants that depend primarily on environment and stress ratio, R.

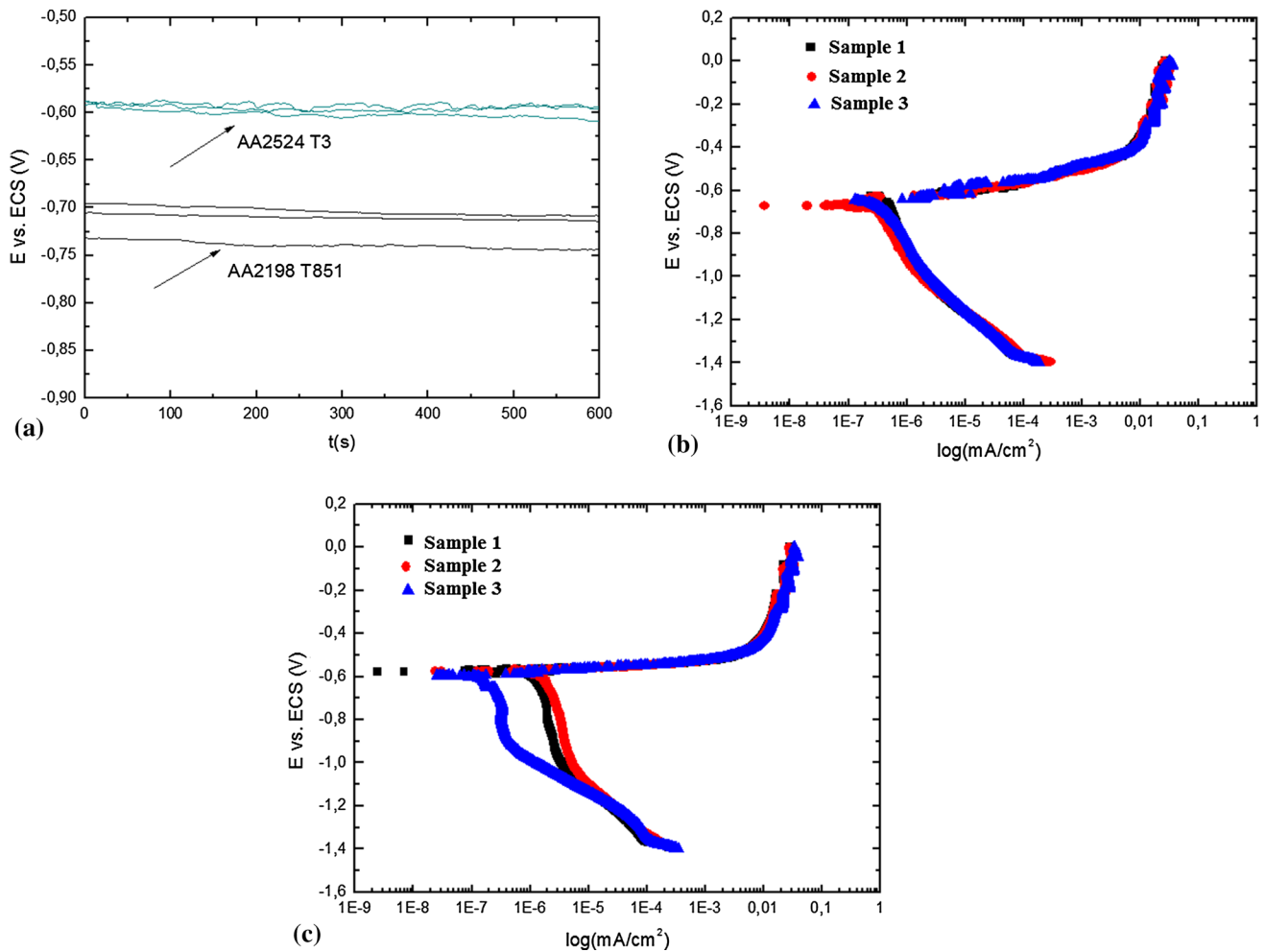


**Fig. 7** Open circuit potential (a) AA2198-T851 and AA2524-T3 alloys (b) and (c) potentiodynamic curves for the AA2198-T851 and AA2524-T3 alloys in aerated  $0.6 \text{ mol L}^{-1}$  NaCl aqueous solution at scan rate of  $0.5 \text{ mV s}^{-1}$

**Table 1** Results of tensile tests for the alloys studied

Properties	AA2524-T3	AA2198-T851
$\sigma_y$ , MPa	$340.3 \pm 2.53$	$438.9 \pm 6.7$
$\sigma_{UTS}$ , MPa	$445.4 \pm 1.5$	$480.0 \pm 7.3$
EL, %	$19.7 \pm 2.0$	$10.3 \pm 5.0$
E, GPa	$70 \pm 2.5$	$75 \pm 1.2$

Table 2 presents the materials parameters from Eq 3, obtained from the linear regression from the data related exclusively to region II, removed from the complete set of data reported in Fig. 8. Figure 9 presents a comparison between the FCG curves modeled by Eq 3 considering the two Al alloys and the air and seawater fog effects.

As can be seen in Table 2, the corrosive medium has affected the FCG rate of both aluminum alloys, in a quite similar way. Comparing the FCG behavior in air and saline environment, it was observed that in both alloys, the  $m$  value remained quite close (2524-T3: 2.99 and 2.33 and 2198-T851: 2.93 and 3.01), while the  $A$  value has slightly increased from  $2.6 \times 10^{-7}$  to  $4.6 \times 10^{-7}$  [(mm/cycle)/(MPa.m<sup>1/2</sup>)<sup>m</sup>] in alloy 2524-T3 and from  $9.1 \times 10^{-8}$  to  $10.2 \times 10^{-8}$  [(mm/cy-

cle)/(MPa.m<sup>1/2</sup>)<sup>m</sup>] in alloy 2198-T851. These effects promoted a higher FCG rate in the case of saline environment in both alloys and a higher FCG rate in alloy 2198-T851.

Considering the seawater fog environment, at each new loading cycle, the corrosion process takes place at the vicinity of the crack tip, where stresses are higher and there is an intense plastic deformation and the formation of slip bands that continuously expose new material layers to the corrosive environment. The resulting micro-cracks from this deformation process break the passive layer on the crack tip surface exposing the metal to the corrosive atmosphere, upon which corrosion is accelerated (Ref 22). Thus, in the seawater fog environment, this process is responsible for the increase in the FCG rate and causes change in the values of  $m$  and  $A$  in both alloys. Therefore, it can be stated that, in the Paris regime, the corrosive environment negatively influences the fatigue behavior of both 2524-T3 and 2198-T851 Al alloys.

The results of corrosion-fatigue presented in this work showed that the 2198-T851 aluminum alloy for a same value of  $\Delta K$  presents a higher FCGR in seawater fog. This may be explained as follows: Pitting corrosion is not referenced in the present research although it can induce stress corrosion cracking (SCC) process. However, with the evolution of the FCG tests in the presence of a corrosive medium, the AA2524-

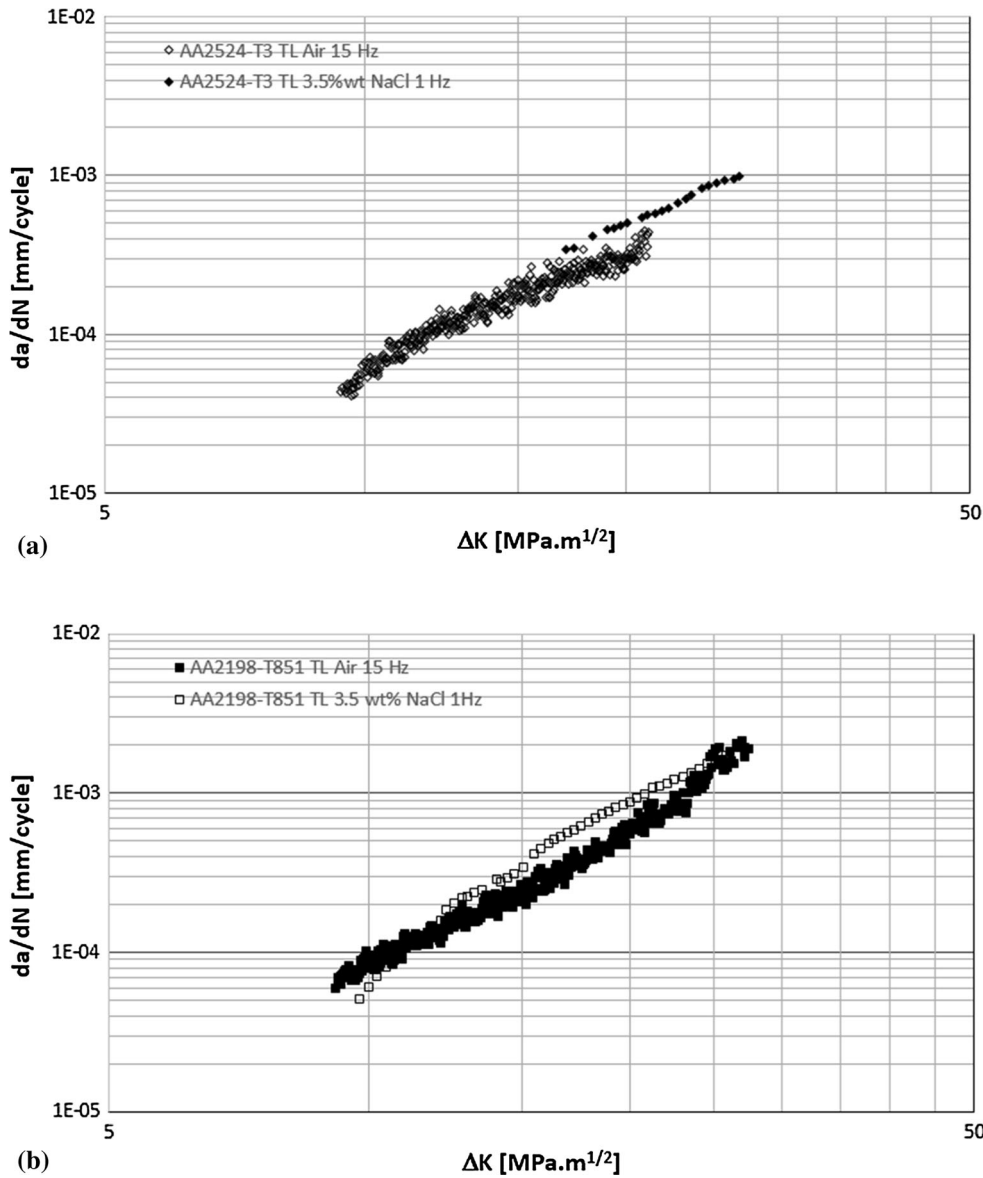


Fig. 8 da/dN vs.  $\Delta K$  curves to threshold obtaining of the alloys (a) AA2198-T851 and (b) AA2524-T3

Table 2 Parameters of Paris equation

	Alloy			
	AA2524-T3		AA2198-T851	
	Air	Seawater Fog	Air	Seawater Fog
Paris's Eq( $R^2$ )	$da/dN = 2.6 \times 10^{-7} (\Delta K)^{2.29} (0.95)$	$da/dN = 2.6 \times 10^{-7} (\Delta K)^{2.29} (0.99)$	$da/dN = 2.6 \times 10^{-7} (\Delta K)^{2.29} (0.98)$	$da/dN = 2.6 \times 10^{-7} (\Delta K)^{2.29} (0.98)$
$m$	2.29	2.33	2.93	3.01
$A, (mm/cycle)/(MPa \cdot m^{1/2})^m$	$2.6 \times 10^{-07}$	$4.6 \times 10^{-07}$	$9.1 \times 10^{-08}$	$10.2 \times 10^{-08}$

T3 aluminum alloy becomes more resistant. Probably, the FCG of the AA2198-T851 aluminum alloys may be associated with the dissolution mechanism of the intermetallic compounds, while the hardening process is the main phenomenon governing the fatigue crack growth for AA2524-T3 aluminum alloy.

The presence of precipitates, such as T1 and  $\theta'$  in the AA2198-T851 alloy, makes an inversion of the corrosion mechanism. At first, these precipitates are anodic with respect to the aluminum matrix, resulting in their dissolution. However, during the corrosion process, as the Li element is preferably

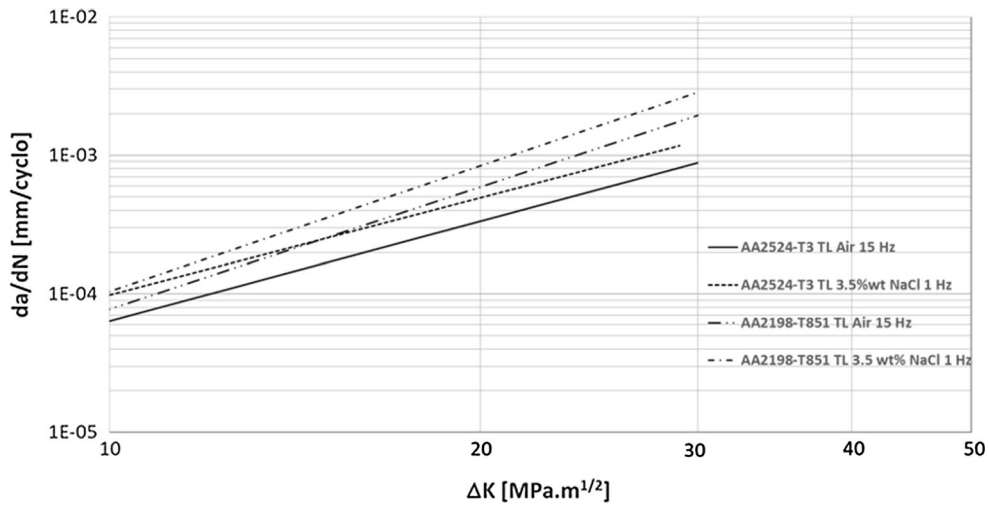


Fig. 9 FCG tests comparison for the 2XXX series alloys in air and seawater fog conditions (region II)

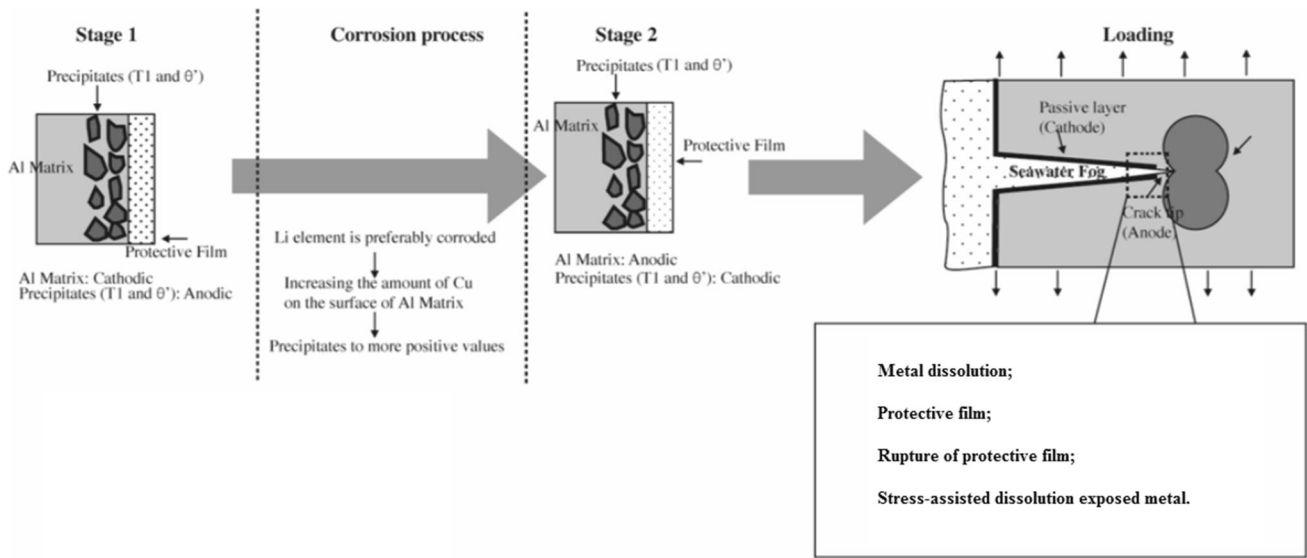


Fig. 10 Schematic drawing of the proposed corrosion-fatigue mechanism for the 2198-T851 aluminum alloy

corroded, there is an increase in the Cu amount on the surface of the aluminum matrix. This leads the precipitates chemical potential to more positive values, becoming cathodic with respect to the rest of the Al alloys, causing now the dissolution of the matrix instead of the precipitates (Ref 23, 24). This dissolution at the crack tip is responsible for the higher FCG rate observed for the 2198-T851 alloy when exposed to the saline environment, when it is compared with the results observed in air. Figure 10 shows a schematic drawing of the proposed corrosion-fatigue mechanism for the 2198-T851 aluminum alloy.

Moreto (Ref 10, 25) studied the corrosion behavior of 2198-T851 and 2524-T3 aluminum alloys using scanning vibrating electrode (SVET) and scanning kelvin probe (SKP) techniques. The results obtained clearly demonstrate a high activity at the first moment of immersion in saline environment, and it was possible to get complementary data supporting the physical interpretations of the galvanic corrosion processes. The localized characteristics of the 2198-T851 and 2524-T3 aluminum

alloys are essentially related to the existence of intermetallic compounds, which, due to their different nature, chemical potential may be cathodic or anodic in relation to the aluminum matrix. As described by Ferreira et al. (Ref 26), the corrosion resistance of aluminum alloys is usually dependent on the metal heterogeneities and/or on the medium or exposure conditions. Another influence of intermetallic compounds on the aluminum matrix is strictly related to their depolarizing effect. In fact, the different composition of the solute-depleted matrix and the solute-rich precipitates produces galvanic cells, leading to the dissolution of the less noble areas (Ref 27). In this way, we may conclude that if the material is to be used without the presence of a crack, the AA2198-T851 alloy presents the best results. However, when we consider the corrosion-fatigue synergy, once the propagation of the crack begins, the AA2524-T3 alloy stands out.

Figure 11 shows the fracture surfaces of the test specimens fatigue tested in seawater fog and analyzed by SEM. The analysis revealed the presence of an oxide layer along the entire



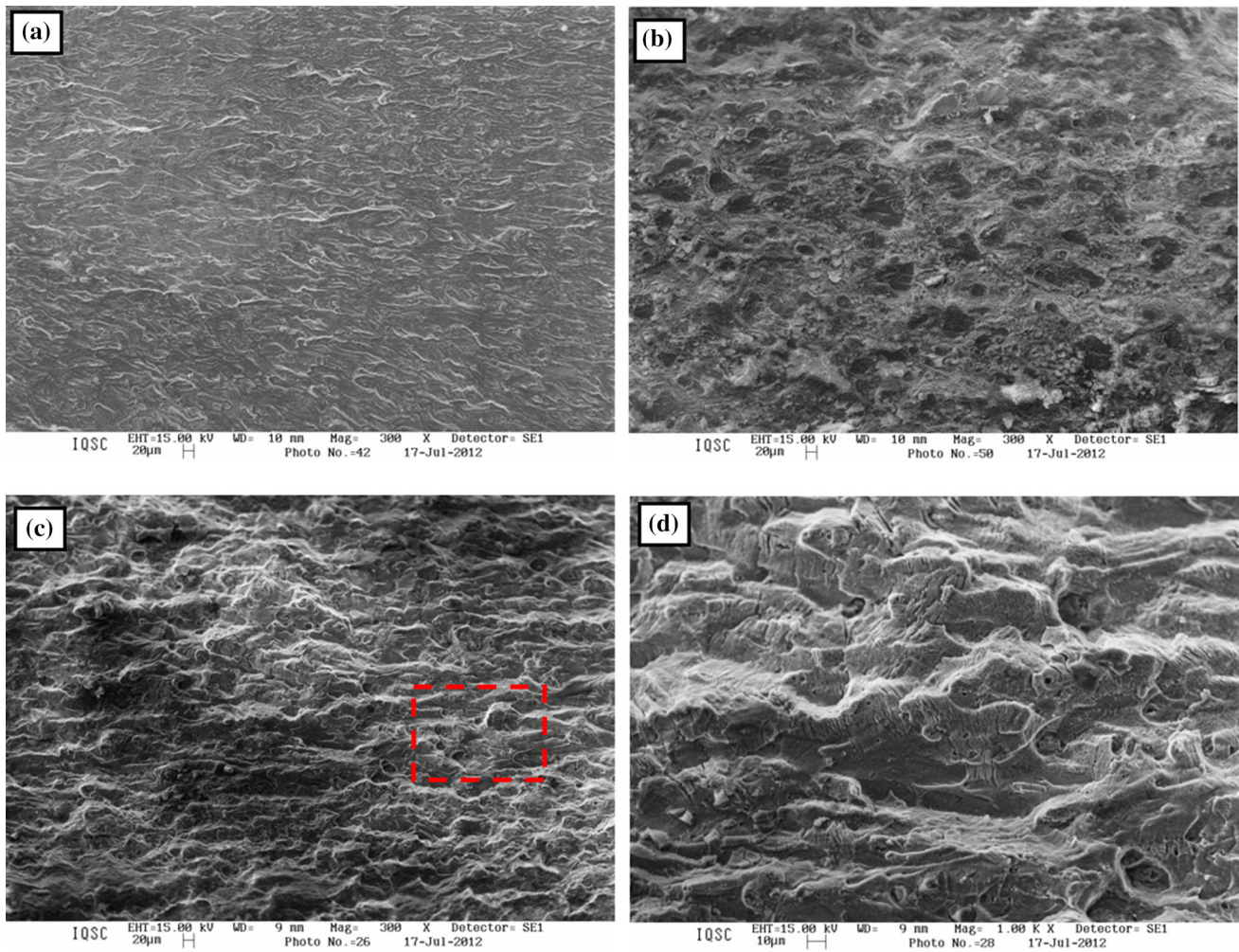


**Fig. 11** SEM fracture surface analysis of FCG in seawater fog environment. General features of regions: AA2198-T851 (a) low  $\Delta K$  and (b) high  $\Delta K$ ; AA2524-T3 alloy (c) low  $\Delta K$  and (d) high  $\Delta K$

surface as a result of the corrosion products, bringing some difficulty for an accurate assessment of the fracture mode. However, it might be noticed that the fracture mode is essentially transgranular and that the fracture surface of AA2198-T851 is quite flat (Fig. 11a), while the AA2524 presented a more sinuous crack path (Fig. 11c). In both cases, it was observed that the transgranular fractures took place by development of striations as result of localized plastic deformation at the crack tip, Fig. 11(d). Lina and Yanga (Ref 28) studying the corrosion fatigue and surface chemistry studies of high strength aluminum alloys, suggested that the hydrogen produced by reactions of water vapor with the freshly formed fracture surface at the crack tip, is responsible for the embrittlement at the processing zone, causing an enhancement in crack growth rate by an active path dissolution mechanism. However, the absence of intergranular fracture or clear regions of cleavage could cast doubt on the explanation of the acceleration of crack based on the mechanism of hydrogen embrittlement (Ref 29).

Liu and Xiong (Ref 30) developed a model to explain the crack propagation in AA2524-T3 and AA7050-T7452 aluminum alloys subjected to fatigue loading, constant-amplitude, and actual random-spectra loading histories at room tempera-

ture (of about 25 °C) and at cryogenic temperature of – 70 °C. In the mentioned work, it was possible to verify that the 2524-T3 aluminum alloy presented transgranular fractures. With regard to the 2198-T851 aluminum alloy, it was possible to notice a much more discrete oxide formation compared to the AA2524-T3 alloy. The process is greatly aided by the action of the medium in both cases.

#### 4. Conclusions

The 2198-T851 (Solution Heat Treated, Cold Worked, and Artificially Aged) aluminum alloy with Li addition was specifically designed to have an improved mechanical and corrosion properties in order to be used as fuselage components in aircrafts, as a possible substitute for the regular Al alloy, such as the AA2524-T3 (Solution Heat Treated and Cold Worked). In this study, we concluded that the localized characteristics of both aluminum alloys are essentially related to the existence of intermetallics, which, due to their different nature, may be cathodic or anodic in relation to the aluminum matrix. The corrosive medium has affected the FCG rate of both aluminum

alloys, in a quite similar way. For both aluminum alloys, the corrosion process took place at the vicinity of the crack tip, where stresses are high and there is intense plastic deformation specially influenced by the slip bands causing micro-cracks that expose new material layers to the corrosive environment. With regard to the 2198-T851 aluminum alloy, the T1 and  $\theta'$  make an inversion of the corrosion mechanisms, causing dissolution of metal and not more of precipitates with the corrosion evolution. This dissolution at the crack tip promotes a higher rate of propagation for the 2198 alloy in seawater fog condition.

## Acknowledgments

The authors gratefully acknowledge the Department of Materials Engineering, University of São Paulo—USP for providing the laboratory facilities and the Brazilian research funding agencies CNPq (Processes: 303684/2015-1 and 402142/2016-0) and CAPES (Process: BEX4936/10-8) for their financial support. The authors would like to express their thanks to Professor Fernando Quites, in memoriam, for the contributions made in this work.

## References

- G.E. Totten and D.S. Mackenzie, *Handbook of Physical Metallurgy and Process*, CRC Press, New York, 2003
- J.A. Moreto, F.A. Paschoal Júnior, C.I.S. Maciel, L.H.C. Bonazzi, J.F. Leoneli Júnior, C.O.F.T. Ruchert, and W.W. Bose Filho, Environmentally-Assisted Fatigue Crack Growth in AA7050-T73511 Al Alloy and AA2050-T84 Al-Cu-Li Alloy, *Mater. Res.*, 2015, **18**(6), p 1291–1297
- ASM International, *ASM SPECIALTY Handbook: Aluminum and Aluminum Alloys in Aluminum-Lithium Alloys*, Ohio, ASM International, 1993, p 121
- B. Decreus, A. Deschams, P. Donnadieu, in *Understanding the Mechanical Properties of 2198 Al-Li-Cu Alloy in Relation with the Intra-Granular and Inter-Granular Precipitate Microstructure*. International Conference on the Strength of Materials. (Book Series: Journal of Physics Conference Series, v.240, Aug. 2009, 2009)
- T. Warner, Recently Developed Aluminium Solutions for Aerospace Applications, *Mater. Sci. Forum*, 2006, **519–521**, p 1271–1278
- O.C. Gamboni, J.A. Moreto, L.H.C. Bonazzi, C.O.F.T. Ruchert, and W.W. Bose Filho, Effect of Salt-Water Fog on Fatigue Crack Nucleation of Al and Al-Li Alloys, *Mater. Res.*, 2013, **17**(1), p 250–254
- Z.Q. Zheng, B. Cai, T. Zhai, and S.C. Li, The Behavior of Fatigue Crack Initiation and Propagation in AA2524-T34 Alloy, *Mater. Sci. Eng. A*, 2011, **528**, p 2017–2022
- T.L. Anderson, *Fracture Mechanics Fundamentals and Applications*, 2nd ed., CRC Press, Boca Raton, 1995
- American Society for Metals, *Metals Handbook*, 9th ed., ASM International, Ohio, 1990
- J.A. Moreto, C.E.B. Marino, W.W. Bose Filho, L.A. Rocha, and J.S.C. Fernandes, SVET, SKP and EIS Study of the Corrosion Behaviour of High Strength Al and Al-Li Alloys used in Aircraft Fabrication, *Corros. Sci.*, 2014, **84**, p 30–41
- American Society for Testing and Materials, *ASTM E8 M: Standard Test Methods for Tension Testing of Metallic Materials*, American Society for Testing and Materials, Philadelphia, 2000
- American Society for Testing and Materials, *ASTM E647: Standard Test Method for Measurement of Fatigue Crack Growth Rates*, American Society for Testing and Materials, Philadelphia, 2008
- ASTM, *ASTM B909-00: Standard Guide for Plane Strain Fracture Toughness Testing of Non-stress Relieved Aluminum Products, Annual Book Of Standards, Section 2—Nonferrous Metal Products, vol. 02.02, Aluminum and Magnesium Alloys*, ASTM, West Conshohocken, 2001, p 614–617
- S.J. Hudak, Jr., A. Saxena, R.J. Bucci, and R.C. Malcolm, *Development of Standard Methods of Testing and Analyzing Fatigue Crack Growth Rate Data—Final Report*, AFML TR 78-40, Air Force Materials Laboratory, Wright Patterson Air Force Base, Dayton, 1978
- P. Cavaliere and A. Santis, Effect of Anisotropy on Fatigue Properties of AA2198 Al-Li Plates Joined by Friction Stir Welding, *Metall. Sci. Technol.*, 2008, **26**(2), p 21–130
- R.C. Souza, in *Efeito do estiramento no comportamento em fadiga da liga de Al 2524-T3*. Congresso Brasileiro de Ciência e Engenharia de Materiais (IPEN, Foz do Iguaçu, 2006)
- R.P. Wei, R.P. Gangloff, in *Fracture Mechanisms: Perspectives and Directions (Twentieth Symposium)*, *ASTM STP 1020*, ed. by R. P. Wei, R. P. Gangloff (American Society for Testing Materials, Philadelphia, 1989), pp. 233–264
- S. Suresh, *Fatigue of Materials*, Cambridge University Press, Cambridge, 1991
- N.E. Dowling, *Mechanical Behavior of Materials*, Prentice Hall Inc., Englewood Cliffs, 1993
- Y.Q. Chen, S.P. Pan, M.Z. Zhou, D.Q. Yi, D.Z. Xu, and Y.F. Xu, Effects of Inclusions, Grain Boundaries and Grain Orientations on the Fatigue Crack Initiation and of 2524-T3 Al alloy, *Mater. Sci. Eng. A*, 2013, **580**, p 150–158
- A. Tzamtzis and A.T. Kermanidis, Improvement of Fatigue Crack Growth Resistance by Controlled Over Aging in 2024-T3 Aluminium Alloy, *Fatigue Fract. Eng. Mater. Struct.*, 2014, **00**, p 1–13
- K. Komai, Corrosion fatigue, *Comprehensive Structural Integrity: Fracture of Materials from Nano to Macro*, R.O. Ritchie and Y. Murakami, Ed., Elsevier, Amsterdam, 2003, p 345–358
- Xu Yue, Xiaojing Wang, Zhaotong Yan, and Jiaxue Li, Corrosion Properties of Light-Weight and High-Strength 2195 Al-Li alloy, *Chin. J. Aeronaut.*, 2011, **24**, p 681–686
- J.F. Li, Simulation on Function Mechanism of T1 (Al<sub>2</sub>CuLi) Precipitate in Localized Corrosion of Al-Cu-Li alloys, *Trans. Nonferrous Met. Soc. China*, 2006, **16**, p 1268–1273
- J.A. Moreto. (2012) Estudo da corrosão e corrosão-fadiga em ligas de Al e Al - Li de alta resistência para aplicação aeronáutica. Tese (Doutorado em Ciência e Engenharia de Materiais) - Ciência e Engenharia de Materiais, Universidade de São Paulo, São Carlos, 2012
- S.C. Ferreira, L.A. Rocha, E. Ariza, P.D. Sequeira, Y. Watanabe, and J. C.S. Fernandes, Corrosion Behaviour of Al/Al<sub>3</sub>Ti and Al/Al<sub>3</sub>Zr Functionally Graded Materials Produced by Centrifugal Solid-Particle Method: Influence of the Intermetallics Volume fraction, *Corros. Sci.*, 2011, **53**, p 2058–2065
- A. Barbucci, G. Bruzzone, M. Delucchi, M. Panizza, and G. Cerisola, Breakdown of Passivity of Aluminium Alloys by Intermetallic Phases in Neutral Chloride Solution, *Intermetallics*, 2000, **8**(3), p 305–312
- C.-K. Lina and S.-T. Yanga, Corrosion Fatigue Behavior of 7050 Aluminum Alloys in Different Tempers, *Eng. Fract. Mech.*, 1998, **59** (6), p 779–795
- N.D. Alexopoulos, E. Migklis, and A. Stylianos, Fatigue Behavior of the Aeronautic Al-Li (2198) Aluminum Alloy Under Constant Amplitude Loading, *Int. J. Fatigue*, 2013, **56**, p 95–105
- J. Xiong, M. Liu, Modelling Crack Propagation in Aluminium-Alloys 2524-T3 and 7050-T7452 Subjected to Fatigue Loading at Low Temperature. Preprints 2016, 2016100066